PERIODICA POLYTECHNICA SER. MECH. ENG. VOL. 46, NO. 2, PP. 159–175 (2002)

THE THERMAL DIFFUSIVITY MEASUREMENT OF ANTHRACITE BY THE FLASH METHOD IN THE GREEN AND CALCINED STATE

Gyula GRÓF[1]

Department for Energy
Budapest University of Technology and Economics
H–1521 Budapest, Hungary
Phone: (36 1) 4632564

Received: March 7, 2001

Abstract

Since introducing of the flash method of thermal diffusivity measurement, a large scale of devices and evaluation methods has been developed with various levels of sophistication. Widening the application field of the method is going on continuously and thanks to the computer technology available today, the evaluation of experiments and the determination of thermal parameters can be performed in the case of non-ideal measurement data. With the help of the classical solution of the heat conduction equation, we give a short analysis of influencing factors like the sample thickness-to-diameter ratio, the heat losses, the effect of the flash duration and prolonged heat penetration on the front side. The knowledge of the anthracite properties is essential in the determination of the thermal characteristics of packed coal beds. Because of the unavailability of these data for coals of different origin, the author's objective was to test whether the flash method is applicable for determining the thermal diffusivity of anthracite. A number of anthracite grains with different size were embedded in acrylic resin and after cutting and polishing we got the proper specimens. Samples were made with layers both parallel and perpendicular to the direction of the energy input. The thermal diffusivities in the parallel and the perpendicular directions are characteristically different. While this difference is only around 30% in the green state, it has been increased to about 300% or more for some samples in the calcined state.

Keywords: flash method, thermal diffusivity, heat penetration.

1. Introduction

According to TAYLOR and MAGLIÇ (1981), the flash method is considered standard among the thermal diffusivity determination procedures. The present measurements were performed by the use of the device using a flashlamp (KISS et al., 1993). The anthracite cannot be used as a specimen in its granular form directly for the flash method. The different sized grains were embedded in acrylic resin and after cutting

[1]The author obtained a three months scholarship from the *Ministère de l'Éducation du Québec* that took place at the *Université du Québec à Chicoutimi* and the measurements were done at the Heat Transfer & Combustion Laboratory of GRIPS (*Groupe de Recherche en Ingénierie des Procédés et Systèmes*).

and polishing we got the proper coin like samples. The evaluation method proposed originally by PARKER et al. (1961) – that is based on the analytical solution of a perfectly insulated sample and ideal pulse ($\kappa = 0.1388 \cdot L^2/t_{1/2}$, where $t_{1/2}$ is the time needed for the rear side temperature to reach 50% of its maximum) did not perform satisfactorily in our case. Most of the rear side temperature histories registered by us were different from those appearing in the literature: a slight continuous increase was observed instead of horizontal or decreasing tendency. We considered that the glass envelope of the flash tube and other solid surfaces re-emit the absorbed energy during the registration, causing a slight increase of the sample temperature. (The same effect could happen in other instruments if the windows of the sample chambers absorb a part of the flash energy.)

Because we did not find the appropriate solution for the temperature distribution in the literature, in the following section we give an analysis covering the effects of different factors like the sample thickness-to-diameter ratio, the heat losses, and the effect of the flash and continuous heat penetration on the front side.

2. Mathematical Analysis

2.1. The Base Solution

The next analysis is based on the separation of the variables, the classical solution method of heat conduction problems. (It is considered that this method shows satisfactory convergence only at longer time, but the given determination of thermal diffusivity uses the least square method for the curve fitting, thus this characteristic is not detrimental.) The thermophysical properties of different substances depend on the temperature, but for small temperature excursions, it is suitable to use the linear heat-conduction equation

$$\kappa \cdot \nabla^2 T(r, z, t) = \frac{\partial T(r, z, t)}{\partial t}, \tag{1}$$

or in dimensionless form

$$\nabla^2 \vartheta(\omega, \xi, Fo) = \frac{\partial \vartheta(\omega, \xi, Fo)}{\partial Fo}, \tag{2}$$

where κ = $\lambda/(\rho \cdot c)$ is the thermal diffusivity, m^2/s;
λ = the heat conductivity, W/(m · K);
c = the specific heat capacity, J/(kg · K);
ρ = the density, kg/m^3;
$T(r, z, t)$ = temperature at point r, z, K;
r, z = coordinates of cylindrical system, m;
t = time, sec;
ω = r/L radial dimensionless coordinate;
ξ = z/L axial dimensionless coordinate;
Fo = $\kappa \cdot /L^2$ dimensionless time.

As it is common, one can obtain the solution of (2) in the following form

$$\vartheta(\omega, \xi, Fo) = \sum_{m=1}^{\infty}\sum_{n=1}^{\infty} C_{m,n} \cdot Z(\beta_m, \xi) \cdot R(\gamma_n, \omega) \cdot e^{-(\beta_m^2+\gamma_n^2)\cdot Fo}. \tag{3}$$

The β_m and γ_n eigenvalues are calculated according to the boundary conditions, and $C_{m,n}$ from the initial condition. We consider that boundary condition of the third kind exists on all surfaces of the sample, $Bi_r = (\alpha_r \cdot L)/\lambda$ and $Bi_z = (\alpha_z \cdot L)/\lambda$, where α_z is the heat transfer coefficient on the front and rear sides of the sample, and α_r is the one along its perimeter. The coin-like specimen has a thickness L and a radius R.

The boundary conditions are

at $\xi = 0$ $(z = 0)$

$$-\frac{\partial\vartheta}{\partial\xi} + Bi_z \cdot \vartheta = 0, \tag{4a}$$

$\xi = 1$ $(z = L)$

$$\frac{\partial\vartheta}{\partial\xi} + Bi_z \cdot \vartheta = 0, \tag{4b}$$

at $\omega = M = (R/L)$ $(r = R)$

$$-\frac{\partial\vartheta}{\partial\omega} + Bi_r \cdot \vartheta = 0, \tag{5}$$

and the initial condition is

at $Fo = 0$

$$\vartheta(\omega, \xi, Fo) = \Omega(\omega, \xi). \tag{6}$$

As one can realize, the heat source term is missing both from the (2) and (4a) equations. We introduce an alternative way to determine the time dependent temperature field caused by the short irradiation of the front side, and this procedure makes the analysis of the pulse time and the heat penetration also possible. We consider (1) independent of r (later analysis will show that if R/L is high enough, then the heat conduction in the radial direction plays no role) and differentiating both sides of (1) with respect to z, we obtain

$$\kappa\frac{\partial^2}{\partial z^2}\left(\frac{\partial T}{\partial z}\right) = \frac{\partial}{\partial t}\left(\frac{\partial T}{\partial z}\right). \tag{7}$$

Substituting the heat flux $\dot{q}_z = -\lambda\partial T/\partial z$

$$\kappa\frac{\partial^2}{\partial z^2}(\dot{q}) = \frac{\partial}{\partial t}(\dot{q}). \tag{8}$$

As it is known, the heat flux satisfies the same differential equation as the temperature, but one should pay attention to the appropriate initial and boundary conditions for $\dot{q}$.

The temperature distribution in a semi-infinite body can be determined as a function of the composite variable $\zeta = z/(2\sqrt{\kappa \cdot t})$. After a stepwise raise of the surface temperature (previously kept uniform, considered as equal to 0) the solution has the next form (see GRIGULL and SANDNER, 1984)

$$T(z, t) = T_w \cdot (1 - \text{erf}\,(\zeta)), \tag{9}$$

where T_w = suddenly applied surface temperature,

$\text{erf}\,(\zeta) = \dfrac{2}{\pi} \displaystyle\int_0^{\zeta} e^{-u^2}\,\mathrm{d}u$, the error function.

Now, we apply solution (9) to determine $\dot{q}$. A uniform temperature field in the sample means $\dot{q} = 0$. Thus, when a constant heat flux is suddenly applied at the front surface for the time period t_f, we obtain the heat flux distribution analogously to (9)

$$-\lambda \frac{\partial T}{\partial z} = \dot{q}_z = \dot{q}_w \cdot \left(1 - \text{erf}\,\left(\frac{z}{2\sqrt{\kappa \cdot t_f}}\right)\right). \tag{10}$$

The temperature distribution in the semi-infinite region is now calculated by partial integration of (10). If, during the flash time period there is no temperature change at the rear side, the sample with finite thickness can be considered as an infinite region.

We obtain the temperature function from (10)

$$T_f(z, t_f) = 2\frac{\dot{q}_w \sqrt{t_f}}{b}\left[\frac{1}{\sqrt{\pi}} e^{-\zeta^2} - \zeta \cdot \text{erfc}\,(\zeta)\right], \tag{11}$$

where: $\text{erfc}\,(\zeta) = 1 - \text{erfc}(\zeta)$, $\zeta = \dfrac{z}{2\sqrt{\kappa \cdot t_f}}$ and

$b = \sqrt{\lambda \rho c}$ is the effusivity of heat (thermal lumped parameter).

The temperature variation at the front surface is

$$T_f(z = 0, t_f) = 2\dot{q}_w \sqrt{\frac{t_f}{\pi \cdot \lambda \cdot \rho \cdot c}}. \tag{12}$$

Let the energy of the flash lamp be = Q. As a rough estimate one can consider that during the t_f period the energy emission is uniform, thus $\dot{q}_w \cong Q/t_f$, and after substitution into (11), the estimated front surface temperature is

$$T_f(z = 0, t_f) = \frac{2 \cdot Q}{\sqrt{t_f \cdot \pi \cdot \lambda \cdot \rho \cdot c}}. \tag{13}$$

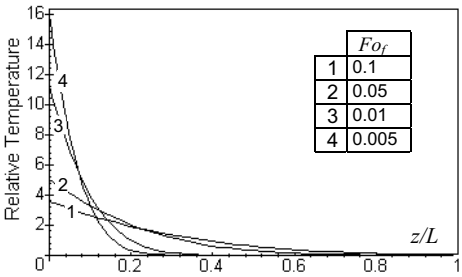

Fig. 1.a. Relative front surface temperature

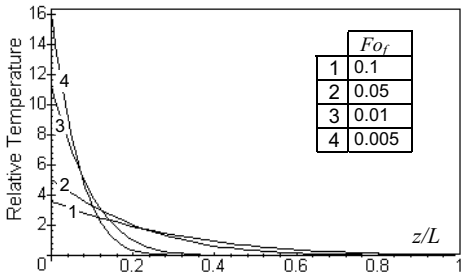

Fig. 1.b. Relative temperature distribution

The final maximum temperature change is $T_{\max} = Q/(L \cdot \rho \cdot c)$ when the sample is adiabatic, thus the relative front surface temperature is (see *Fig.1.a*)

$$\vartheta_f(Fo_f, \xi = 0) = \frac{2}{\sqrt{Fo_f}} \cdot \frac{1}{\sqrt{\pi}},$$

the dimensionless temperature distribution in the specimen is (see *Fig.1.b*)

$$\vartheta_f(\xi) = \frac{2}{\sqrt{Fo_f}} \cdot \left[\frac{1}{\sqrt{\pi}} e^{-\frac{\xi^2}{4 \cdot Fo_f}} - \frac{\xi}{2\sqrt{Fo_f}} \operatorname{erfc}\left(\frac{\xi}{2\sqrt{Fo_f}} \right) \right], \tag{14}$$

where

$$\vartheta_f = \frac{T_f}{T_{\max}}, \qquad Fo_f = \frac{\kappa \cdot t_f}{L^2}, \qquad \xi = \frac{z}{L}.$$

Following the above-presented way, a more detailed description can be developed, paying attention to the time variation of the irradiation by the flash lamp. Applying an instantaneous heat flux at the front surface of a semi-infinite body, the $\dot{q}_0(z, t)$ distribution can be determined by differentiating (10)

$$\dot{q}_0(z, t) = \frac{e^{-\frac{z^2}{4at}} a \cdot z}{2\sqrt{\pi}\,(a \cdot t)^{3/2}}. \tag{15}$$

Hence, in case of an arbitrary $g(t)$ shape function the heat flux distribution will be

$$\dot{q}_g(z, t) = \int_0^t g(t - \tau) \cdot \dot{q}_0(z, \tau)\, \mathrm{d}\tau. \tag{16}$$

Finally, at time t_f the temperature distribution can be calculated as

$$T(z, t = t_f) = \int_0^z \dot{q}_g(u, t = t_f)\, \mathrm{d}u. \tag{17}$$

It is shown that, within the duration of the input pulse, the temperature distribution builds up according to (14) – or more generally according to (17). If we use this temperature distribution as an initial condition, the temperature history can be described as a simple equalization that happens according to the boundary conditions. The solution for the heat conduction problem mentioned above, neglecting the details, is as follows – see details at ÖZISIK (1980).

The separated solutions for ξ and ω direction are, respectively

$$Z(\beta_m, \xi) = \beta_m \cdot \cos(\beta_m \cdot \xi) + Bi_z \sin(\beta_m \cdot \xi), \tag{18}$$

$$R(\gamma_n, \omega) = J_0(\gamma_n \cdot \omega). \tag{19}$$

The calculation of the eigenvalues that appear in (18) and (19) is based on the boundary conditions. Substituting the eigenfunction (18) into (4a) it is readily seen that independently of the values of Bi and β_m, it is true. So substituting (18) into (4b), and (19) into (5), one gets the following transcendental equations, respectively

$$\cot(\beta_m) = \frac{1}{2}\left(\frac{\beta_m}{Bi_z} - \frac{Bi_z}{\beta_m}\right), \tag{20}$$

$$\gamma_n \cdot J_1(\gamma_n \cdot M) + Bi_r \cdot J_0(\gamma_n \cdot M) = 0, \tag{21}$$

$$M \cdot \gamma_n \cdot J_1(\gamma_n \cdot M) + Bi_R \cdot J_0(\gamma_n \cdot M) = 0. \tag{22}$$

where $Bi_R = M \cdot Bi_r = \frac{R}{L}\frac{\alpha L}{\lambda} = \frac{\alpha R}{\lambda}$, and J_0, J_1 are the BESSEL functions.

Some of the first roots of (20) and (19) can be found in the literature, i.e. ÖZISIK (1980), GRIGULL (1984), or can be found with the help of powerful numerical tools available nowadays.

(It is easy to see that only the first root depends really on the values of Bi numbers. For the small value of β the $\cot(\beta)$ can be substituted with $1/\beta$, hence $\beta_1 \approx \sqrt{Bi^2 + 2Bi}$. Because small values of Bi numbers appear in the realistic measurement conditions when $m = 2$, the values of β_m / Bi will increase rapidly, so the second term at the right side of (17) can be omitted. Also, it is derivable from the left side of (20) that for $m = 2$, $\beta_m \approx (m-1) \cdot \pi$ is a good approximation. The same effect appears in (22), as values of γ_n increase the terms at the left side are more and more different, so the eigenvalues can be calculated as the roots of $J_1(M \cdot g_n) = 0$ for $n >= 2$.)

Since the separated eigenfunctions are orthogonal, one can rewrite (3) into the following form

$$\vartheta(\omega, \xi, Fo) = Z(\xi, Fo) \cdot R(\omega, Fo), \tag{23}$$

where

$$Z(\xi, Fo) = \sum_{m=1}^{\infty} C_{z,m} \cdot Z(\beta_m, \xi) e^{-\beta_m^2 \cdot Fo},$$

$$R(\omega, Fo) = \sum_{n=1}^{\infty} C_{r,n} \cdot R(\gamma_n, \omega) e^{-\gamma_n^2 Fo}.$$

The initial condition (6) can be rewritten as

$$\vartheta(\omega, \xi, Fo = 0) = Z(\xi, Fo = 0) \cdot R(\omega, Fo = 0). \tag{24}$$

As above let

$$Z(\xi, Fo = 0) = \frac{2}{\sqrt{Fo_f}} \left[\frac{1}{\sqrt{\pi}} e^{-u^2} - u \cdot \operatorname{erfc}(u) \right], \tag{25a}$$

where $u = \dfrac{\xi}{2\sqrt{Fo_f}}$ and

$$R(\omega, Fo = 0) = 1. \tag{25b}$$

Eqs. (25a), (25b) hold the following assumptions:

- the energy irradiation is constant during the t_f time period
- the energy distribution does not vary in the r direction

(It is worth to mention that the whole analysis can be made without the above restrictions.) $C_{z,m}$ and $C_{r,n}$ are calculated from the next formulas:

$$C_{z,m} = \frac{1}{N_z(\beta_m)} \int_0^1 Z(\xi, Fo = 0) \cdot Z(\beta_m, \xi)\, \mathrm{d}\xi, \tag{26}$$

$$C_{r,n} = \frac{1}{N_r(\gamma_n)} \int_0^M R(\omega, Fo = 0) \cdot R(\gamma_n, \omega)\, \mathrm{d}\omega, \tag{27}$$

where

$$N_z(\beta_m) = \frac{1}{2}(\beta_m^2 + Bi^2) \left(1 + \frac{Bi}{\beta_m^2 + Bi^2} + Bi \right), \tag{28}$$

$$N_r(\gamma_n) = \frac{1}{2} J_0^2(\gamma_n) \cdot M^2 \cdot \left(1 + \frac{Bi_R^2}{\gamma_n^2} \right). \tag{29}$$

It should be emphasized, that the Fo number appearing in (23) is equal to 0 at the end of the flash duration, so the time elapsed from the starting of the flash is $t + t_f$.

The calculated temperature field, the front and rear side temperature histories are shown in *Fig. 2.a* and *Fig. 2.b* for the case of $Fo_f = 0.05$ and $Bi = 0.001$. Several calculations were performed to compare the above solution with those that appear in the literature. The most frequent problem investigated is the finite pulse

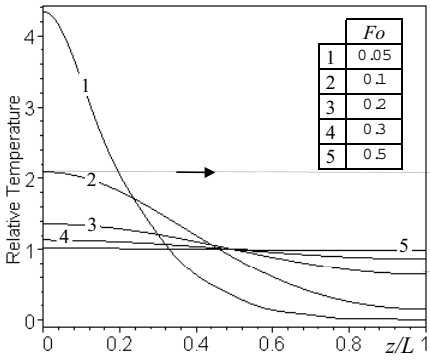

Fig. 2.a. Relative temperature distribution

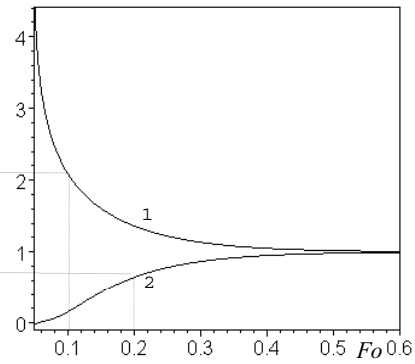

Fig. 2.b. Relative front (1) and rear (2) surface temperature history

time effect. For example, the flash shape function, proposed by LARSON and KOYAMA (1967), is

$$\dot{q}(t) = \frac{Q \cdot t}{t_p^2} \cdot \exp\left(-\frac{t}{t_p}\right). \tag{30}$$

Its maximum appears at $t = t_p$, $\dot{q}_{\max} = \frac{Q}{t_p}\exp(-1)$. Considering the flash irradiation with $\dot{q}_{\max}$ intensity within t_f duration, then the next equation can be derived for t_f : $\frac{Q}{t_f} = \frac{Q}{t_p}\exp(-1)$, hence, $t_p = 0.3679 \cdot t_f$ or $Fo_p = 0.3679 \cdot Fo_f$. Using the above substitution, we found an excellent numerical match between our calculations and the result of LARSON and KOYAMA (1967), p. 470. Obviously, it is limited within the validity of the applied mathematical models.

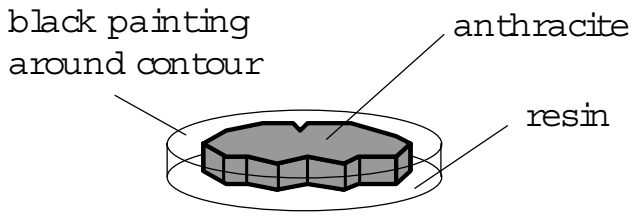

Fig. 3. Typical structure of the prepared specimen

As it was mentioned earlier, the anthracite samples were embedded into a

disc form acrylic resin (see *Fig. 3*), so we need to determine the limits of the applicability of the one-dimensional (z direction) solution. The impact of using the resin is twofold:

- as small diameters are used, the critical diameter problem arises
  (It is known from insulation techniques, that, in case of diameters smaller than $2 \cdot \lambda/\alpha$, increase of insulation thickness causes the increase of heat losses.)
- if the resin absorbs a sufficient amount of energy, its temperature history will follow closely that of the anthracite if there is not a big difference in their thermophysical properties.
  (The used resin was transparent, so we used a black paint around the sample contour.)

Fig.4.a and *Fig. 4.b* give the limits for the R/L ratio when a one-dimensional temperature field can be used in the centre region (i.e. with diameter = $2L$, L) of the sample. As the specimens heat conductivity decreases, the Bi number increases and as it is shown even in the case of an unrealistically high Bi number, the use of a sample with $R/L > 5$ makes the application of the one-dimensional model possible. In other words, one does not need a cylindrical specimen.

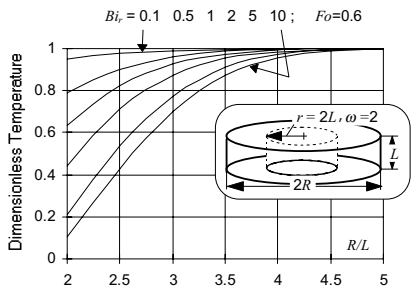

Fig. 4.a. Dimensionless temperature at $\omega = 2$ point

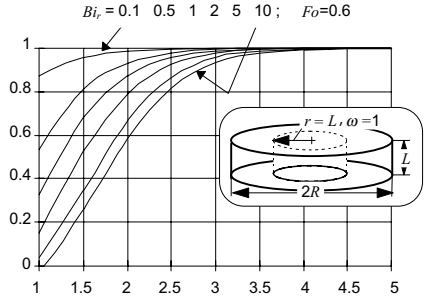

Fig. 4.b. Dimensionless temperature at $\omega = 1$ point

2.2. *Effect of the Continuous Irradiation*

Due to the limited time we had to accomplish the measurements, the repetition rate of the flash was quite high. The glass-tube of the flash lamp itself and the reflector surfaces remained hot for longer and longer periods, and their temperature rose higher and higher in small steps. As a certain temperature level was reached, a

continuous increase of the sample temperature appeared. In the following, we give the analysis for that case similarly to the method used above.

Although the temperature of the flash tube and its surrounding change, the time period that the sample needs for equalization of its temperature is short, hence, we can consider that those hot surfaces can be characterized by a T_f steady temperature. Let the area of the mentioned surfaces be A_f. The heat flux to the sample front surface can be derived from the STEFAN – BOLTZMANN radiation law

$$\dot{Q}_{f,s} = A_s \cdot \varepsilon_{f,s} \cdot \sigma_0 \left[T_f^4 - T^4(r, z = 0, t) \right], \tag{31}$$

where σ_0 = $5.67 \cdot 10^{-8}$ W/(m^{2}K^4) is the STEFAN – BOLTZMANN constant
A_s = sample front surface area, m^2
$\varepsilon_{f,s} = \left(\frac{1}{\varepsilon_s} + \frac{A_s}{A_f} \left(\frac{1}{\varepsilon_f} - 1 \right) \right)^{-1}$ total emissivity.

In the general case of $A_s / A_f \ll 1$, so $\varepsilon_{f,s} = \varepsilon_s$, where ε_s is the emissivity of the sample surface.

The solution satisfying the exact boundary condition described by (31) (non homogeneous, non linear, non time independent) can be obtained with the help of the integral transformation methods. However, as the objective of the present analysis is to find a model that describes the slight increase of the rear side temperature, we can follow a simpler way. Generally, the temperature changes are around 1 K at the rear side in our flash apparatus. As it was shown in the previous chapter, the front side temperature decreases rapidly for a short initial period, then changes slowly for the remaining time of the temperature equalization. The variation of the temperature at this period is also limited to around $1 \div 2$ K. Instead of using the exact condition described by (31), we consider that the continuous heat flux is absorbed on the front surface of the specimen. According to this hypothesis the boundary equations are as follows

at $\xi = 0$

$$-\frac{\partial \vartheta}{\partial \xi} + Bi_z \cdot \vartheta = \frac{L}{\lambda} \dot{q}_f, \tag{32}$$

at $\xi = 1$

$$\frac{\partial \vartheta}{\partial \xi} + Bi_z \cdot \vartheta = 0. \tag{33}$$

The solution can be obtained as the sum of the solution of a steady-state problem and the solution of a homogeneous transient problem:

$$\vartheta(\xi, Fo) = \vartheta_h(\xi, Fo) + \vartheta_s(\xi). \tag{34}$$

The steady-state problem for $\vartheta_s(\xi)$ is

$$\frac{\mathrm{d}^2}{\mathrm{d}\xi^2} \vartheta(\xi) = 0, \tag{35}$$

and the boundary condition
at $\xi = 0$

$$-\frac{\partial \vartheta}{\partial \xi} + Bi_z \cdot \vartheta = \frac{L}{\lambda}\dot{q}_f, \tag{36}$$

at $\xi = 1$

$$\frac{\partial \vartheta}{\partial \xi} + Bi_z \cdot \vartheta = 0. \tag{37}$$

The homogeneous problem for $\vartheta(\xi, Fo)$ is

$$\nabla^2 \vartheta(\omega, \xi, Fo) = \frac{\partial \vartheta(\omega, \xi, Fo)}{\partial Fo}, \tag{38}$$

and the boundary condition
at $\xi = 0$ $(z = 0)$

$$-\frac{\partial \vartheta}{\partial \xi} + Bi_z \cdot \vartheta = 0, \tag{39}$$

$\xi = 1$ $(z = L)$

$$\frac{\partial \vartheta}{3\xi} + Bi_z \cdot \vartheta = 0, \tag{40}$$

the initial condition

$$\vartheta_h(\xi, Fo = 0) = \vartheta_f(\xi, Fo_f) - \vartheta_s(\xi). \tag{41}$$

The form of the solution will be

$$\vartheta_h(\xi, Fo) = \sum_{m=1}^{\infty} C_{z,m} \cdot Z(\beta_m, \xi) \cdot e^{-\beta_m^2 \cdot Fo}. \tag{42}$$

The $\vartheta_f(\xi, Fo_f)$ function describes the temperature distribution in the sample existing at the end of the pulse duration. The eigenfunctions, eigenvalues and $C_{z,m}$ are obtainable similarly as it was shown previously. The boundary conditions (39), (40) are identical to (4a), (4b), (5) thus the eigenvalues are identical, too.

The steady-state problem can be readily solved by the simple integration of the boundary condition and in term of $T_{\max}$ it will be

$$\vartheta_s(\xi) = \frac{\dot{q}_f \cdot L^2}{Q \cdot \kappa} \cdot \frac{\frac{1}{Bi} + 1 - \xi}{2 + Bi}. \tag{43}$$

The theoretical temperature distribution as well as the rear side temperature history is calculated for different conditions. Some results are shown in *Fig.5*. The slope of the temperature history depends on two dimensionless values $S_q = \dot{q}_f \cdot L^2 / Q \cdot \kappa$ and the Bi number.

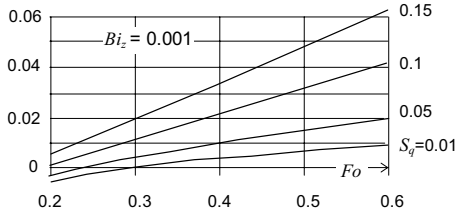

Fig. 5. Relative temperature difference obtained from the 'ideal' solution

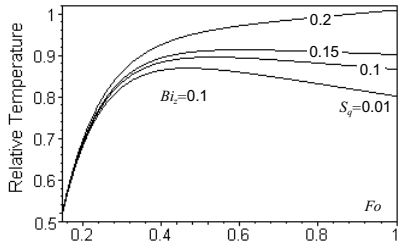

Fig. 6. Relative temperature rise in case of different S_q

As it is known from the literature and it turns out from our calculation as well, when certain deviations from the ideal condition are limited, even in case of multiply effects, the different temperature response curves follow well the ideal curve proposed by PARKER et al. (1961) around $t_{1/2}$. (The course of the rear side temperature depends on the combination of Bi_z and S_q values, and the different values can cause decreasing, increasing or horizontal path. See *Fig.6*).

2.3. Evaluation Procedure

The determination of the thermal diffusivity is based on the curve fitting with the use of the least-square-error (LSE) method. Due to a slight increase of the temperature response the curve fitting is localized to the $1/2 \cdot t_{1/2} - 2 \cdot t_{1/2}$ time range. As it is apparent from the previous section, the deviation from the ideal solution is negligible in the above range, hence we reproduce the measured curve, represented by $(t_n - U_n)$ data pairs with the proper set of A and κ values. A is the value of the ideal amplitude and κ is the value of the thermal diffusivity we want to determine, and U_n is the amplified signal of the thermocouple. The LSE method means that we have to find the minimum of the following function $M(A, \kappa)$

$$M(A, \kappa) = \sum_{j=1}^{n} [U_j - A \cdot V(t_j, \kappa)]^2. \tag{44}$$

It means, one has to solve the set of coupled equations

$$\underline{m}(A, \kappa) = \begin{bmatrix} \dfrac{\partial M}{\partial A} = 0 \\ \dfrac{\partial M}{\partial \kappa} = 0 \end{bmatrix}. \tag{45}$$

Using the NEWTON–RAPHSON procedure (i.e., see KORN (1975)) we need to calculate the JACOBI matrix of (44)

$$\underline{J} = \begin{bmatrix} \dfrac{\partial^2 M}{\partial A^2} & \dfrac{\partial^2 M}{\partial A \partial \kappa} \\ \dfrac{\partial^2 M}{\partial \kappa \, \partial A} & \dfrac{\partial^2 M}{\partial \kappa^2} \end{bmatrix}. \tag{46}$$

If we have $\underline{X}_0[A_0 \ \kappa_0]$ an approach of the solution of (44) is close enough to the $\underline{X}_s = [A_s \ \kappa_s]$ solution, then the next series will tend to $\underline{X}_s$

$$X_i - \underline{J}^{-1} \cdot \underline{m}(\underline{X}_i) = \underline{X}_{i+1}. \tag{47}$$

As the convergence of (47) is very sensitive to $\underline{X}_0$ the evaluation program, running on a PC, checks always the change of the value of $M(A, \kappa)$ as the new $\underline{X}_{i+1}$ is calculated. (The $V(t_j, \kappa)$ (infinite series) was substituted by its first six terms.)

3. Experiments and Results

3.1. Preparation of the Samples

The natural (granular) form of the anthracite cannot be used directly as the specimen for the flash method. Grains of different size and structure were chosen randomly, in order to get the representative value of the thermal diffusivity. The grains were embedded in acrylic resin with the help of a thin walled plastic tube. After cutting and polishing we got the numbers of samples depending on the volume of the embedded grain. Two types of samples were made according to the layered structure of the anthracite: parallel and perpendicular orientation to the direction of the flash (see *Fig. 7*).

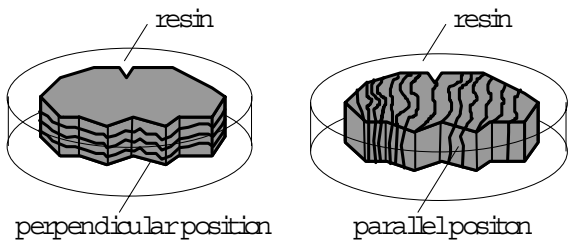

Fig. 7. Positions of the layered structure

3.2. Measuring and Data Acquisition

The rear side temperature history was measured by thermocouples. In order to achieve good signal-to-noise ratio, the preamplifier unit was battery operated and a Fluke handheld, battery operated, digital storage scope meter was used as the A/D and storage unit. The collected data (512 points) were read via RS232 to the PC. A typical registered temperature response together with the fitted ideal curve are shown in *Fig. 8*. According to what was said previously, the curve fitting is localized only to the $1/2 \cdot t_{1/2} - 2 \cdot t_{1/2}$ region.

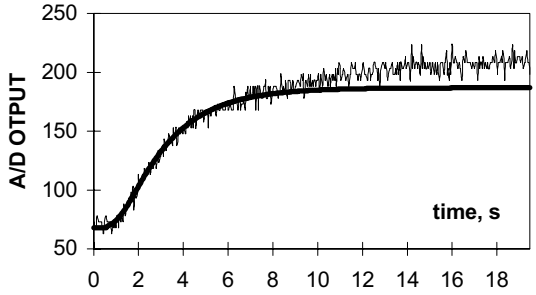

Fig. 8. Typical collected data & fitted curve

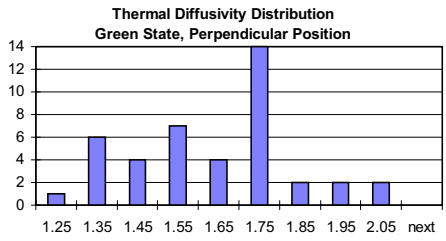

Fig. 9.

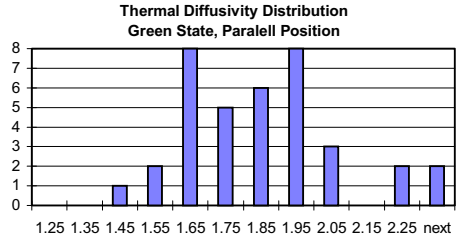

Fig. 10.

3.3. Results

Table 1 – *Table 4* contain the measured values of thermal diffusivity and *Fig.9* – *12* show their distribution. A characteristic difference exists between the parallel and the perpendicular direction. While this difference was only around 30% in the green state, when calcined it increased to app. 300% or even more for some samples. The anisotropy due to the layered structure is more pronounced in the calcined state. The structure is not formed of perfectly parallel, planar layers. Therefore, a precise

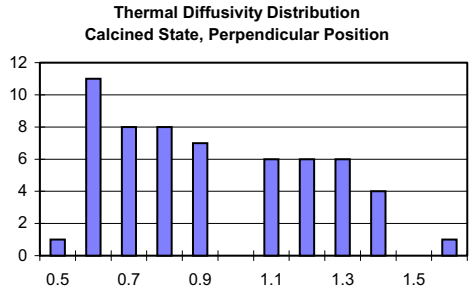

Fig. 11.

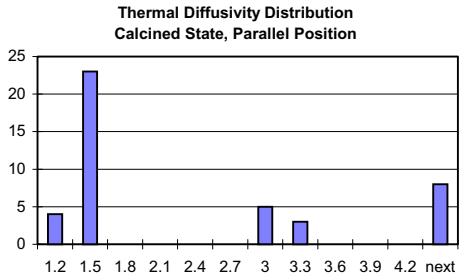

Fig. 12.

Table 1.

Green, Perpendicular, Measured Thermal Diffusivity, $\cdot 10^{-7}$, m^2/s						
Sample	1	2	3	4	5	6
	1.652	1.708	1.339	1.419	1.514	1.759
	1.775	1.624	1.284	1.473	1.486	1.654
	1.692	1.728	1.281	1.397	1.524	1.726
	1.706	1.657	1.272	1.904	1.447	1.890
	1.737	1.583	1.286	1.591	1.540	
	1.703	1.674	1.262	1.603	1.485	
	1.735	1.680	1.236			
	1.718		1.351			
Mean	1.715	1.665	1.289	1.565	1.499	1.757

Statistic			
Spreading	0.186	Minimum	1.310
Standard error	0.076	Maximum	1.845
Mean	1.582		

parallel orientation for some samples could not be performed. Due to the combined influence of the anisotropy and the 'non–perfect' orientation, the scattering appears in *Fig. 11* and even stronger in *Fig. 12*.

3.4. Conclusions

The classical solution by separation of the variables served the analysis of non-ideal rear side temperature histories in the flash measurements. The small deviations from the ideal conditions have significant effect on the course of temperature history only

Table 2.

Green, Parallel, Measured Thermal Diffusivity, $\cdot 10^{-7}$, m^2/s						
Sample	7	8	9	10	11	12
	1.435	1.555	1.599	1.684	1.968	2.152
	1.580	1.592	1.625	1.763	1.870	1.957
	1.606	1.556	1.602	1.704	1.863	1.986
	1.893	1.667	1.868	1.836	2.275	1.753
	1.864	1.717	1.884	1.842	2.187	1.829
		1.651	1.942	1.907	2.280	1.834
Mean	1.676	1.623	1.753	1.789	2.074	1.919

Statistic			
Spreading	0.166	Minimum	2.074
Standard error	0.068	Maximum	0.166
Mean	1.806		

Table 3.

Calcined, Perpendicular, Measured Thermal Diffusivity, $\cdot 10^{-6}$, m^2/s										
Sample	1	2	3	4	5	11	12	13	14	15
Cut 1	0.679	1.333	0.782	1.228	0.718	0.851	0.598	0.686	0.521	1.103
	0.674	1.344	0.783	1.257	0.803	1.035	0.613	0.798	0.523	1.073
	0.690	1.320	0.785	1.232	0.803	1.016	0.542	0.793	0.516	1.118
	0.693	1.345	0.795	1.245	–	1.021	0.563	–	–	1.146
Cut 2	0.563	1.110	0.884	1.231	0.644	–	–	–	–	–
	0.570	1.099	0.878	1.145	0.637	–	–	–	–	–
	0.498	1.124	0.889	1.204	0.546	–	–	–	–	–
	0.515	1.083	0.894	–	0.786	–	–	–	–	–
Mean	0.610	1.220	0.836	1.220	0.705	0.981	0.579	0.569	0.520	1.110

Statistic			
Spreading	0.2853	Minimum	0.5204
Standard error	0.0902	Maximum	1.2657
Mean	1.8396		

at longer time thus applying the localized ideal curve fitting reduces the uncertainty of determination of thermal diffusivity.

Table 4.

Calcined, Parallel, Measured Thermal Diffusivity, $\cdot 10^{-6}$, m^2/s									
Sample	7	8	9	10	16	18	19	20	6
Cut 1	1.217	1.312	1.295	2.866	1.215	4.393	5.178	1.352	1.445
	1.219	1.316	1.299	2.713	1.239	4.305	5.187	2.896	1.432
	1.235	1.313	1.287	3.179	1.215	5.139	5.188	2.871	1.437
Cut 2	1.229	0.813	1.281	3.213	1.245	5.060	5.460	1.376	1.425
	1.244	0.818	–	–	–	–	–	–	–
	1.240	1.048	–	–	–	–	–	–	–
Mean	1.231	1.103	1.291	2.993	1.229	4.724	5.253	2.124	1.435

Statistic			
Spreading	1.6026	Minimum	1.1033
Standard error	0.5342	Maximum	5.2532
Mean	2.3758		

References

[1] GRIGULL, U. – SANDNER, H., *Heat Conduction*, Berlin, Springer Verlag, 1984, pp. 71–79.

[2] KISS, L. I. – FALL, B. – CHARETTE, A. – BUI, R. T., Experimental Study of Thermophysical Properties of Solids, *Proceedings of the International Symposium on Development of Application of Ceramic, CIM* 1993, pp. 143–154.

[3] KORN, G. A. – KORN, T. M., *Mathematical Handbook for Scientists and Engineers*, Budapest, Műszaki Könyvkiadó, 1975. (Hungarian translation) pp. 649–651.

[4] LARSON, K. B. – KOYAMA, K., Finite-Pulse-Time Effects in Very Thin Samples Using the Flash Method of Measuring Thermal Diffusivity, *Journal of Applied Physics*, **37** No. 2, (1967), pp. 465–474.

[5] ÖZISIK, M. N., *Heat Conduction*, New York, J. Wiley and Sons, pp. 83–143.

[6] PARKER, W. J. – JENKINS, R. J. – BUTLER, C. P. – ABOTT, G. L., Flash Method of Determining Thermal Diffusivity, Heat Capacity and Thermal Conductivity, *Journal of Applied Physics*, **32** No. 9, (1961), pp. 1679–1684.

[7] TAYLOR, R. E. – MAGLIÇ, K. D., *Compendium of Measurement of Thermophysical Properties*, Plenum Press, New York, 1984, Volume 1, pp. 305–336.